All-optical switch with 1 ps response time enabled by graphene oxide infiltrated subwavelength grating waveguide

Xiaochuan Xu[*a], Zeyu Pan[b], Baohua Jia[c], Yaguo Wang[d], and Ray T. Chen[*b]
[a]Omega Optics, Inc., 8500 Shoal Creek Blvd, Austin, TX 78757, USA;
[b]Department of Electrical and Computer Engineering, The University of Texas at Austin, 10100 Burnet Rd, MER 160, Austin, TX 78758, USA;
[c]Centre for Micro-Photonics, Swinburne University of Technology, Hawthorn, Victoria 3122, Australia
[d]Department of Mechanical Engineering, The University of Texas at Austin, Austin, TX 78712, USA
* xiaochuan.xu@omegaoptics.com; chenrt@austin.utexas.edu

ABSTRACT

In this paper, we propose an all-optical switch using graphene oxide (GO) infiltrated subwavelength grating (SWG) waveguide. Benefiting from the extremely large Kerr coefficient of GO (four orders of magnitude larger than conventional materials) and large mode volume overlap factor of the SWG (4~10 times larger than conventional strip waveguides), the switch is capable of achieving THz speed with less than 1 fJ energy consumption per bit, which is more than three orders of magnitude smaller than THz switches reported so far.

Keywords: subwavelength grating waveguide, graphene oxide, all-optical switch, silicon photonics

1. INTRODUCTION

Driven by bandwidth hungry technologies such as online video and cloud computing, the skyrocketing growth of global data traffic has no sign of halting. As the desire for large bandwidth permeates optical interconnects such as core networks and data centers, electronic switches must be abandoned when speed is beyond 100 Gbps. To accommodate the bandwidth demand, all-optical switches must be adopted in the near future. Silicon photonics has been receiving considerable applications in recent years.[1, 2] The high refractive index of silicon can minimize footprint and maximize bandwidth density, and the mature silicon electronics fabrication technology can be leveraged to massively produce photonic devices at a low cost. However, two-photon absorption and free carrier absorption induced loss degrades the switches' performance. Hybrid integration of third-order nonlinear materials is a promising alternative, but its performance is limited by the small mode volume overlap between the third-order nonlinear material and the optical mode. In the meantime, 2D materials have been showing amazing optical properties and revolutionizing the conventional devices.[3] In this paper, we propose an all-optical switch using GO infiltrated SWG waveguide. Benefiting from the extremely large Kerr coefficient of GO (four orders of magnitude larger than conventional materials) and large mode volume overlap factor of the SWG waveguide (4~10 times larger than conventional strip waveguides), the switch is capable of achieving THz speed with less than 1 fJ energy consumption per bit, which is more than three orders of magnitude smaller than THz switches reported so far.

2. NONLINEARITY OF GRAPHENE OXIDE

A high quality GO film is essential in high performance photonic devices. GO sheets can be deposited on virtually any substrates in the form of thin films using techniques such as drop-casting, dip-coating, spraying, spin-coating, electrophoresis, Langmuir–Blodgett (L–B)/Langmuir–Schaefer and transfer via vacuum-filtration. Control over film uniformity, surface morphology, thickness, and surface coverage depend on the deposition methods and parameters employed. Drop-casting, dip-coating, and spraying often result in nonuniform deposition due to the aggregation of GO, allowing poor control over the film thickness and roughness. Once deposited, the van der Waals forces are sufficient to keep the GO sheets strongly adhered to the substrate. Individual sheets are held together with strong hydrogen bonding, which also helps the films adhere to hydrophilic surface.

Silicon Photonics XII, edited by Graham T. Reed, Andrew P. Knights, Proc. of SPIE Vol. 10108, 1010805
© 2017 SPIE · CCC code: 0277-786X/17/$18 · doi: 10.1117/12.2252640

Downloaded From: http://proceedings.spiedigitallibrary.org/pdfaccess.ashx?url=/data/conferences/spiep/91354/ on 06/06/2017 Terms of Use: http://spiedigitallibrary.org/ss/term

In the vacuum-filtration approach, GO flakes are synthesized by the chemical reduction of graphite via a modified Hummers method. Firstly, graphite and $NaNO_3$ are mixed with concentrated H_2SO_4. By vigorous stirring, the reducing agent –$KMnO_4$ is added into the suspension. Then H_2O_2 is added into the mixture at 98 ^oC. The product is washed and dried, and then the GO sheets are obtained after the purification. The obtained GO flakes are dispersed in deionized water by ultrasonication and centrifuge to achieve a clear yellow suspension of exfoliated GO. The GO suspension is vacuum-filtrated through a mixed cellulose ester film (Millipore) with 25 nm pores.[4] Then the free-standing GO thin films were transferred to the glass substrates. The surface roughness of the GO thin film is well controlled below 50 nm by reducing the layer numbers of the GO flakes in the solution. Figure 1a shows the optical microscope images of the GO film on a 125 μm thick cover glass. Wrinkles have been clearly observed, which increase the overall surface roughness of the GO film. Atomic Force Microscope (AFM) confirms that the surface roughness is around 34 nm, as shown in Figure 1b. The area between wrinkles has a surface roughness of ~17 nm, which is 50% lower than the overall surface roughness.

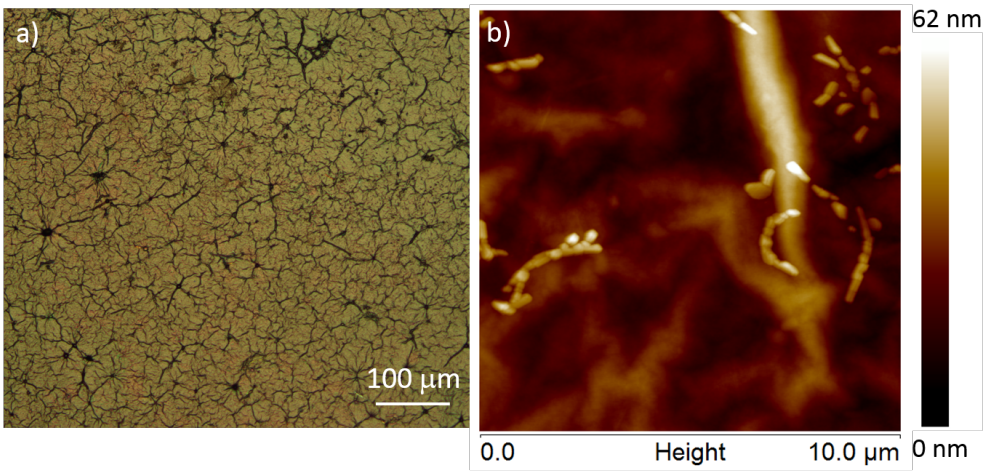

Figure 1 The optical microscope a) and AFM images b) of the GO film formed by filtering and transfer.

Z-scan has been considered as one of the most effective methods to investigate the nonlinear optical characteristics of thin films.[5] With a single Gaussian laser beam in a tight focus geometry, the transmittance of a nonlinear medium through a finite aperture in the far field as a function of the sample position z measured with respect to the focal plane. Assume, for instance, a material with a positive nonlinear refractive index and a thickness smaller than the diffraction length of the focused beam (a thin medium). This can be regarded as a thin lens of variable focal length. Starting the scan from a distance far away from the focus, the beam irradiance is low and negligible nonlinear refraction occurs; hence the transmittance remains constant. As the sample is brought closer to focus, the beam irradiance increases, leading to self-lensing in the sample. A negative self-lensing prior to focus will tend to collimate the beam, causing a beam narrowing at the aperture which results in an increase in the measured transmittance.[5]

Figure 2 shows the z-scan system. Light is collimated through a 7 mm collimator (Thorlab, F810FX-1550). A half wave plate (HWP, Thorlab WPH10M-1550) converts circular polarization into linear polarization. A quarter wave plate (QWP, Thorlab WPG10M-1550) is used to rotate the linear polarization direction.[6] Together with the 50:50 polarization dependent splitter cube (PDS, Thorlab CM1-PBS254), the quarter wave plate is used as a tunable attenuator to control the irradiance. Another 90:10 polarization independent splitter (PIS, Thorlab BS030) is used to split 10% of the total power for system monitoring to avoid the fake nonlinear signals.[7] An f = 60 mm bi-convex lens (Thorlab LB1723-C) is used to focus the light beam. The sample is mounted on a motorized stage (Thorlab MTS25-Z8E). A 50:50 plate beam splitter (PBS, Thorlab BSW12R) is used to split the beam into two channels, open and close. In the open channel, an f = 60 mm bi-convex lens (Thorlab LB1723-C) is used to ensure the collection of all the power in this channel. A photodiode (PD#2 Newport 818IR) is exploited to monitor the power. To ensure the photodiode works at the linear response range, a 10x attenuator is mounted in front of PD#2. In the close arm, an Iris aperture and another f=60 mm bi-convex lens (Thorlab LB1723-C) are used to harvest all the light passing through the aperture. PD #3 is used to detect the power in the close arm. The signals from PD #1~3 are collected with a BNC board (National Instrument BNC2110) and PCI card (National Instrument PCIe-6321). A labview program is developed to synchronize the

Downloaded From: http://proceedings.spiedigitallibrary.org/pdfaccess.ashx?url=/data/conferences/spiep/91354/ on 06/06/2017 Terms of Use: http://spiedigitallibrary.org/ss/term

movement of the motorized stage and data collection. The image of the real system is shown in Figure 2b and c. Calmar femtosecond laser with a pulse width of 67 *f*s and a repetition rate of 20 MHz is used as the light source. The spectrum of the pulse is ~ 40 nm wide and centered at 1560 nm. Since the surface roughness of the GO is large compared to semiconductor materials, e.g. silicon, a continuous-working (CW) laser is exploited as a low irradiance source for background scattering subtraction. [5]

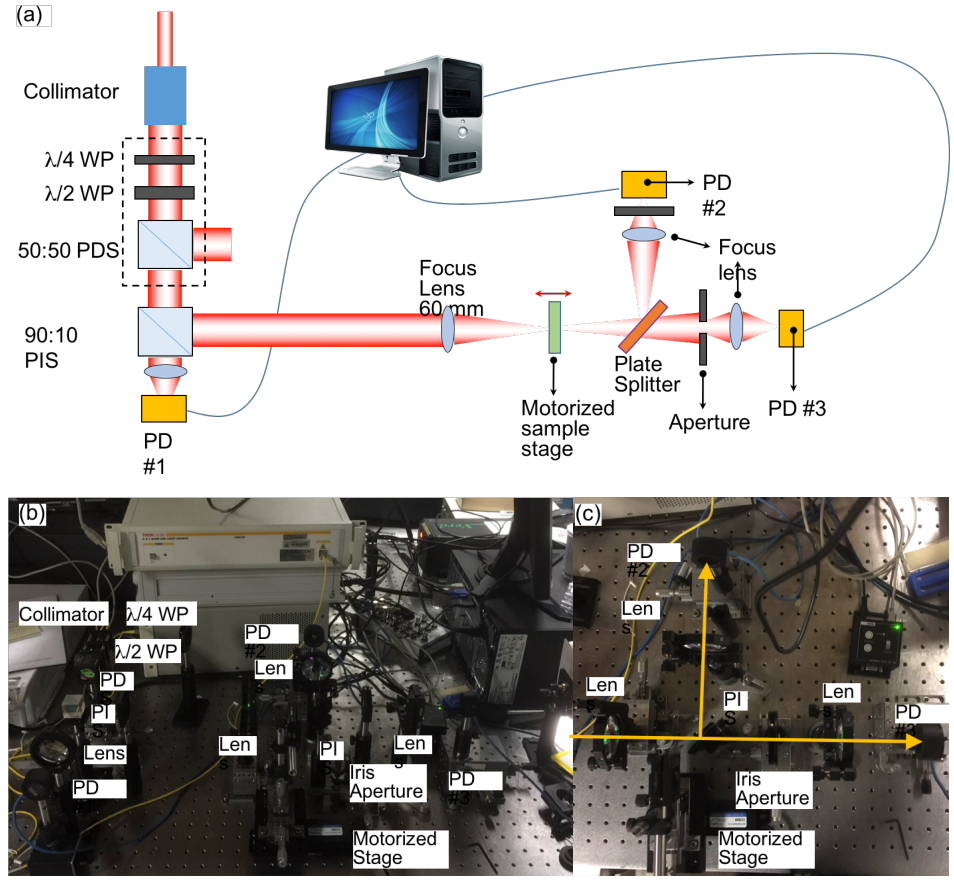

Figure 2 (a) Z-scan system illustration. (b) The z-scan setup built in Phase I. (c) The open and close aperture channel in the z-scan system. WP: waveplate. PDS: polarization dependent splitter. PIS: polarization independent splitter. PD: Photodetector.

In the set-up, the Gaussian beam diameter w_0 at the focus is 16.9 μm and the Rayleigh range z_0 is 580 μm, defined as $z_0 = \pi w_0^2 / \lambda$. The scanning range needs to be larger than $\pm 5 z_0$, corresponding to 5.8 mm in total. A 1 μm thick GO film is formed by the vacuum-filtration method and transferred onto a 125 μm thick cover glass slide. The sample is mounted on a sample holder which can control the tilting of the sample and make its surface perpendicular to the Gaussian beam propagation direction. Figure 3 shows the open and close z-scan curves under different irradiance. In the open aperture channel, the GO film shows a saturable absorption (SA) under 0.3 GW/cm^2, as shown in Figure 3a. When the irradiance increases, the SA becomes less eminent, indicating the existence of excited state absorption (ESA). When the irradiance increases to 4.3 GW/cm^2, multi-photon absorption starts to happen, showing a dip in the open aperture z-scan. In the close arm, when the irradiance is ~0.3 GW/cm^2, the GO film shows a positive n_2 of 2.9x10^{-13} m^{2}W^{-1}, as shown in Figure 3b, which is more than four orders of magnitude larger than a-Si, c-Si, and SiN, as summarized in Table 1. An interesting phenomenon has been observed that the third-order nonlinearity induced focus and defocus abate as the irradiance increases, as shown in Figure 3b. When the irradiance increases to 4.3 GW/cm^2, the z-scan curve changes into a shape indicating the existence of negative n_2, as shown Figure 3b. The thermal effect might become eminent when the irradiance is high.

Downloaded From: http://proceedings.spiedigitallibrary.org/pdfaccess.ashx?url=/data/conferences/spiep/91354/ on 06/06/2017 Terms of Use: http://spiedigitallibrary.org/ss/term

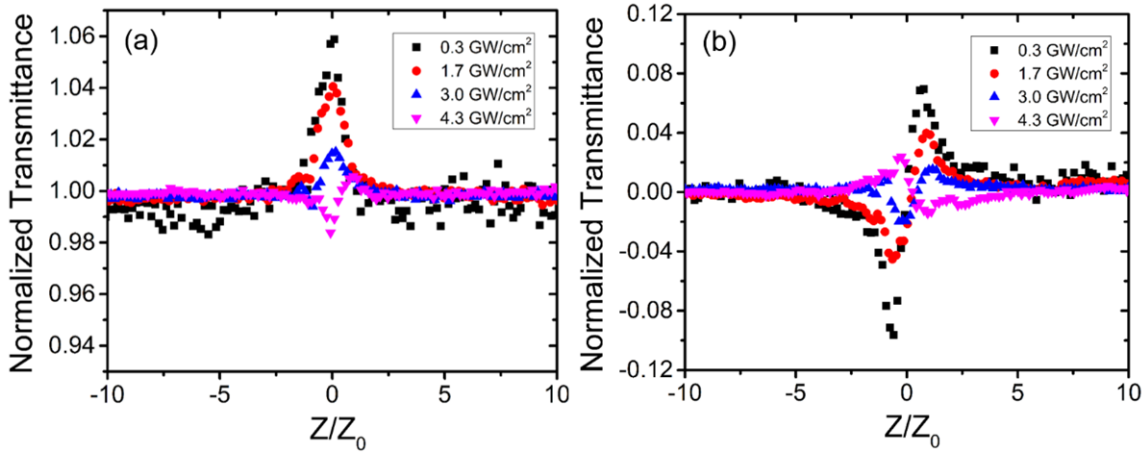

Figure 3 The Z-scan curves from (a) open aperture and (b) close aperture measurements under different irradiance at the focus position.

Table 1 The nonlinear optical coefficient of different materials

	a-Si	c-Si	SiN	GO	rGO	GO
Wavelength	1550nm	1550nm	1550nm	800 nm	800 nm	1550 nm
n_2 (m^2W^{-1})	1.82×10^{-17}	4.55×10^{-18}	2.6×10^{-19}	7.5×10^{-13}	$\sim1.5\times10^{-12}$	2.9×10^{-13}
β (cm GW^{-1})	0.25	0.9		4×10^4	$\sim4\times10^4$	-
FOM	5	0.3	>>1	1	4.56	>>1

3. SUBWAVELENGTH GRATING WAVEGUIDE

Micro-ring resonators on the SOI platform have been considered as a basic building block for a vast range of applications [8]. To further improve the performance of conventional ring resonators, there is growing interest in SWG ring resonators (SWGRRs) [9, 10]. However, the quality factor of SWGRR decreases rapidly as its radius reduces due to the increasing bend loss from the curved SWG waveguides. The bend loss is primarily caused by the scattering induced by surface roughness and the radiation loss due to small curvature. Through conformal transferring analysis, we found that the radiation loss can be significantly reduced by properly designing the equivalent refractive index profile and shifting the delocalized mode back to the center of SWGs. Ideally, to eliminate the mode delocalization after conformal transformation, the effective refractive index profile in cylinder coordinate system should follow:

$$n_{\text{eff}}(\rho) = \begin{cases} n_{\text{cl}} r_2 / \rho & \rho < r_1 \ , \ \rho > r_2 \\ n_{\text{co}} r_2 / \rho & r_1 \le \rho \le r_2 \end{cases} \tag{1}$$

Here, n_{cl} and n_{co} are the effective refractive indices of the waveguide cladding and core, respectively. r_1 and r_2 are the radius of the inner and outer edges of the bend, respectively. Since a large portion of a guided mode is concentrated in the high index region, the distortion due to the cladding refractive index can be safely ignored and the mode distortion can be minimized by engineering the SWGs. We proposed to use the trapezoidal shape silicon pillars instead of conventional rectangular silicon pillars, as shown in Figure 4a. The refractive index along the radical direction can be tuned through adjusting the top (W_a) and bottom (W_b) base of the silicon pillars.

Downloaded From: http://proceedings.spiedigitallibrary.org/pdfaccess.ashx?url=/data/conferences/spiep/91354/ on 06/06/2017 Terms of Use: http://spiedigitallibrary.org/ss/term

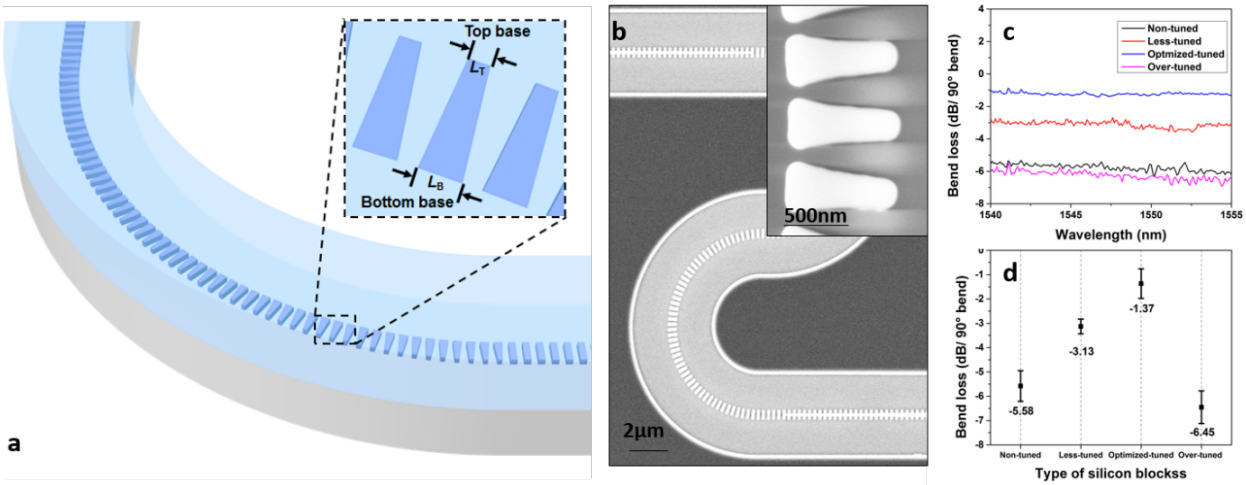

Figure 4 (a) 3D schematic of SWG waveguide bend built with trapezoidal silicon pillars. (b) SEM image of a typical device. Inset: SEM images of optimally tuned silicon pillars. (c) Transmission spectra of the four types of silicon pillars. (d) Statistical insertion loss of the four types of silicon pillars.

To prove the theoretical analysis, four types of silicon pillars: rectangle (W_a= W_b=150nm), under-tuned trapezoid (W_a= 120 nm and W_b= 190 nm), optimally-tuned trapezoid (W_a= 70 nm and W_b= 210 nm) and over-tuned trapezoid (W_a= 140 nm and W_b= 210 nm) have been fabricated. The width and period of the waveguides are 500 nm and 300 nm, respectively. The SEM images of the fabricated bends are shown in Figure 4b. Each device has four 90° bends. The devices are tested in a customized grating coupler alignment system [11-13]. Figure 4c shows the transmission spectra of the four SWG waveguide bends between 1540 nm and 1555 nm for quasi-TE polarization. The insertion loss of the four representative bends at 1550 nm is summarized in Figure 4d, where the optimized trapezoidal silicon pillars is as low as 1.37 dB per 90° bend, only 24.5% of that of the non-tuned rectangular silicon pillars (5.58 dB per 90° bend). Compared to the earlier demonstration of 10 μm SWG bend [10], we are able to reduce the bend radius to 5 μm without increasing the insertion loss. When the pillars are over-tuned, the refractive index distortion and mode mismatch increase, and thus the loss increases.

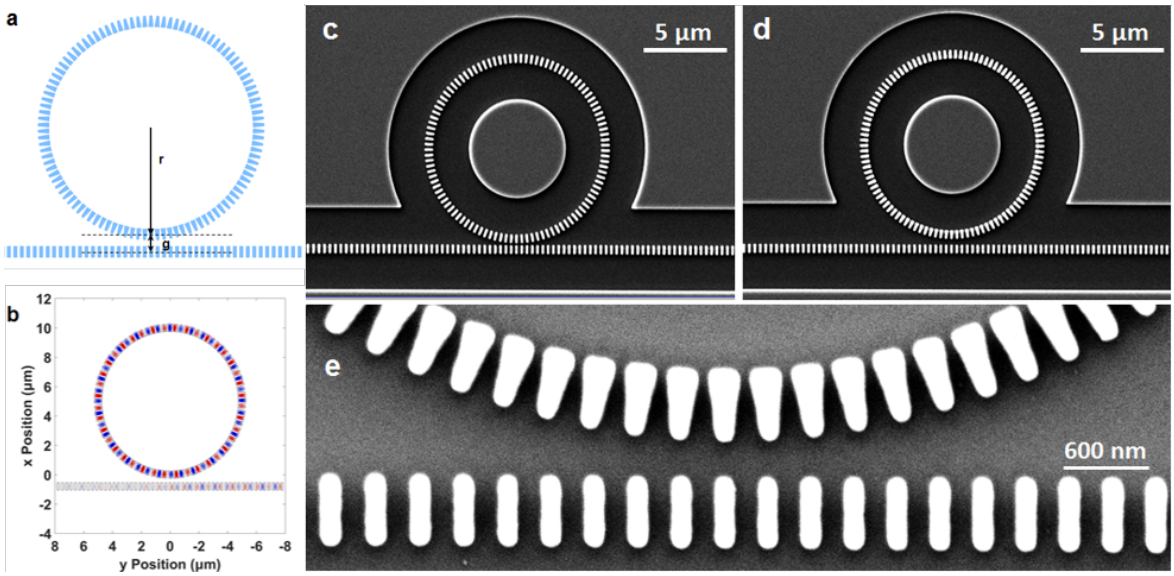

Figure 5 (a) Schematic of a typical SWGRR. (b) Typical top-view of the optical field in an SWGRR on resonance. SEM images of typical 5 μm SWGRR with (c) trapezoidal silicon pillars and (d) rectangular silicon pillars. (e) Coupling region of a 5 μm SWGRR with trapezoidal silicon pillars.

Downloaded From: http://proceedings.spiedigitallibrary.org/pdfaccess.ashx?url=/data/conferences/spiep/91354/ on 06/06/2017 Terms of Use: http://spiedigitallibrary.org/ss/term

Based on the innovation, we designed a 5 μm SWGRR with W_a= 140 nm and W_b= 210 nm. To compare other groups' results, we also designed and fabricated 10 μm SWGRR with trapezoidal silicon pillars. Conventional rectangular 5 μm and 10 μm micro-ring resonators are fabricated on the same chip for comparison. Figure 5a and b show the top view and the THz component of the optical field of an SWGRR on resonance. The SEM images of the fabricated SWGRRs are shown in Figure 5c-e. Figure 6 shows the transmission spectra of the four types of SWGRRs for quasi-TE polarization around the peak has the largest quality factor. The 5 μm SWGRR with trapezoidal silicon pillars can offer a resonance peak with a quality factor as high as 11,500, which is 4.6 times of the highest quality factor (~2,800) resonance peak that a 5 μm SWGRR with conventional rectangular silicon pillars can offer. For 10 μm radius, the SWGRR with trapezoidal silicon pillars can offer a resonance peak with a quality factor as high as 45,000, which is 3 times to our in-house control group (quality factor~15,000).

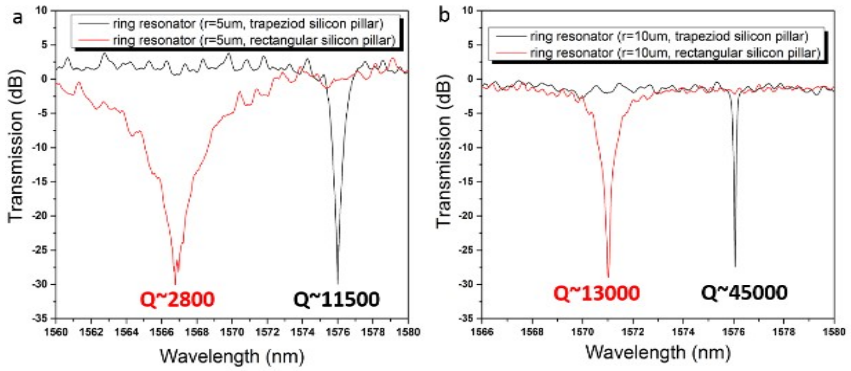

Figure 6 Optical Transmission spectra. (a)SWGRR with a 5 μm radius. (b) SWGRR with a 10 μm radius.

In summary, we observed an n_2 of 2.9×10^{-13} m^2W^{-1} from GO thin films formed by vacuum-filtration. Besides, we have successfully fabricated a 5 μm radius SWGRR with a quality factor of 11,500, which is the smallest SWGRR that have been demonstrated so far. The quality factor of SWGRRs with larger radius can also be improved with the same approach. We experimentally demonstrated a 10 μm SWGRR with a quality factor up to 45,000. Compared to our in-house control group of optimized SWGRR with conventional rectangular silicon pillars, the quality factors increase 4.6 times for 5 μm micro-ring resonators and 3 times for 10 μm micro-ring resonator, respectively.

ACKNOWLEDGMENT

The authors would like to acknowledge the support by the United States Department of Energy (DOE) Small Business Innovation Research (SBIR) program (DE-SC0013178).

REFERENCES

[1] H. Subbaraman, X. Xu, A. Hosseini *et al.*, "Recent advances in silicon-based passive and active optical interconnects," Optics Express, 23(3), 2487-2511 (2015).
[2] X. Xu, H. Subbaraman, J. Covey *et al.*, "Colorless grating couplers realized by interleaving dispersion engineered subwavelength structures," Optics letters, 38(18), 3588-3591 (2013).
[3] H. Dalir, Y. Xia, Y. Wang *et al.*, "Athermal Broadband Graphene Optical Modulator with 35 GHz Speed," ACS Photonics, 3(9), 1564-1568 (2016).
[4] G. Eda, G. Fanchini, and M. Chhowalla, "Large-area ultrathin films of reduced graphene oxide as a transparent and flexible electronic material," Nature Nanotechnology, 3(5), 270-274 (2008).
[5] M. Sheikbahae, A. A. Said, T. H. Wei *et al.*, "Sensitive Measurement of Optical Nonlinearities Using a Single Beam," Ieee Journal of Quantum Electronics, 26(4), 760-769 (1990).

Downloaded From: http://proceedings.spiedigitallibrary.org/pdfaccess.ashx?url=/data/conferences/spiep/91354/ on 06/06/2017 Terms of Use: http://spiedigitallibrary.org/ss/term

[6] X. Q. Yan, Z. B. Liu, X. L. Zhang *et al.*, "Polarization dependence of Z-scan measurement: theory and experiment," Optics Express, 17(8), 6397-6406 (2009).
[7] H. Yan, and J. S. Wei, "False nonlinear effect in z-scan measurement based on semiconductor laser devices: theory and experiments," Photonics Research, 2(2), 51-58 (2014).
[8] W. Bogaerts, P. De Heyn, T. Van Vaerenbergh *et al.*, "Silicon microring resonators," Laser & Photonics Reviews, 6(1), 47-73 (2012).
[9] V. Donzella, A. Sherwali, J. Flueckiger *et al.*, "Design and fabrication of SOI micro-ring resonators based on sub-wavelength grating waveguides," Optics Express, 23(4), 4791-4803 (2015).
[10] V. Donzella, A. Sherwali, J. Flueekiger *et al.*, "Sub-wavelength grating components for integrated optics applications on SOI chips," Optics Express, 22(17), 21037-21050 (2014).
[11] Z. Wang, H. Yan, S. Chakravarty *et al.*, "Microfluidic channels with ultralow-loss waveguide crossings for various chip-integrated photonic sensors," Optics Letters, 40(7), 1563-1566 (2015).
[12] X. C. Xu, H. Subbaraman, S. Chakravarty *et al.*, "Flexible Single-Crystal Silicon Nanomembrane Photonic Crystal Cavity," Acs Nano, 8(12), 12265-12271 (2014).
[13] X. C. Xu, H. Subbaraman, J. Covey *et al.*, "Complementary metal-oxide-semiconductor compatible high efficiency subwavelength grating couplers for silicon integrated photonics," Applied Physics Letters, 101(3), 031109 (2012).

Downloaded From: http://proceedings.spiedigitallibrary.org/pdfaccess.ashx?url=/data/conferences/spiep/91354/ on 06/06/2017 Terms of Use: http://spiedigitallibrary.org/ss/term